

# Anticorrosion Agents for Carbon Steel in Acidic Environments: Synthesis and Quantum Chemical Analysis of New Schiff Base Compounds with Benzylidene

Hamdy Khamees Thabet, Jwahr M. AlGhamdi, Hoda A. Mohammed, Mahmoud A. M. Elsaid, and Ashraf M. Ashmawy\*



Cite This: *ACS Omega* 2023, 8, 39770–39782



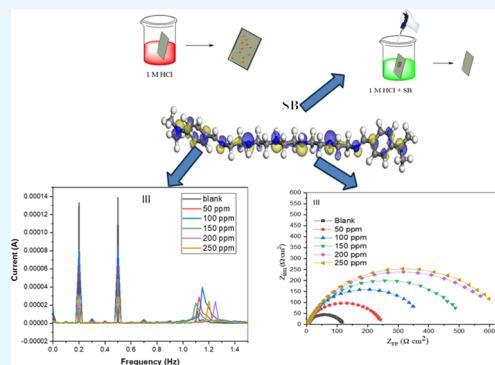
Read Online

ACCESS |

Metrics & More

Article Recommendations

**ABSTRACT:** Novel Schiff bases (SBs), namely,  $N_1, N_2$ -bis(2-(((E)-4-chlorobenzylidene)amino)ethyl)ethane-1,2-diamine (I),  $N_1, N_2$ -bis(2-(((E)-4-(dimethylamino)benzylidene)amino)ethyl)ethane-1,2-diamine (II), and  $N_1, N'_1$ -(ethane-1,2-diyl)bis( $N_2$ -(((Z)-4-dimethylamino)benzylidene) amino)methylethane-1,2-diamine (III), were prepared and characterized by using elemental analysis, IR, and  $^1\text{H}$  NMR spectroscopy. For assessing carbon steel in diverse settings, with and without inhibitors at varying concentrations, electrochemical frequency modulation (EFM), electrochemical impedance spectroscopy (EIS), and potentiodynamic polarization (PP) techniques were employed. The results showed that the synthesized inhibitors effectively decreased the corrosion rate of carbon steel in acidic media and the inhibition efficiency reached up to 93% for compound III at a concentration of 250 ppm. In addition, all prepared compounds were successful as anticorrosion agents, and the inhibition mechanism followed chemisorption from the Langmuir isotherm. The data obtained from the theoretical analysis show that the efficiency of the prepared compounds was in the order  $\text{III} < \text{II} < \text{I}$ . Furthermore, quantum chemical calculations were performed to gain insight into the electronic structure of the compounds. The analysis of the highest occupied molecular orbital (HOMO) and the lowest unoccupied molecular orbital (LUMO) showed that compound III had the highest surface coverage due to its specific molecular structure and spacer. This observation agreed well with the Langmuir adsorption data.



## INTRODUCTION

Carbon steel is widely acknowledged as a preferred material for electrochemical, power generation, and chemical industries due to its cost-effectiveness and corrosion-resistant alloys. However, its inferior corrosion resistance necessitates a thorough investigation of corrosion processes in different environments. To counter this issue, various approaches, such as coatings, cathodic protection, and corrosion inhibitors, have been employed to prevent corrosion.<sup>1,2</sup> Understanding the corrosion mechanisms fully is crucial to effectively address specific corrosion problems with each protective technique.<sup>3–5</sup> Corrosion of carbon steel in acidic media is a persistent challenge faced by various industries, impacting the structural integrity and longevity of the equipment and infrastructure. As a result, the search for efficient anticorrosion inhibitors has been the subject of significant research.<sup>6–8</sup>

In this context, novel Schiff base compounds have emerged as promising candidates with the potential to provide robust protection against corrosion in acidic environments.<sup>9–17</sup> The compound, characterized by the general formula  $\text{R}-\text{C}=\text{N}-\text{R}'$ , where R and R' represent aryl, alkyl, cycloalkyl, or heterocyclic groups resulting from the combination of an amine and a

carbonyl group, shows promise as an inhibitor. Various Schiff bases (SBs) have been documented as efficient corrosion inhibitors for mild steel<sup>9–14,18–23</sup> and aluminum<sup>12,13</sup> in acidic environments. Currently, numerous Schiff bases (SBs) are utilized as a solution to address the corrosion issue. For instance, Sengupta et al.<sup>5</sup> synthesized three Schiff bases, namely, 2-(2-hydroxybenzylideneamino)phenol (Inh-1), 2-((2-hydroxyphenylimino)methyl)-4-methylphenol (Inh-2), and 2-((2-hydroxyphenylimino)methyl)-4-methoxyphenol (Inh-3). The corrosion inhibition efficiency of these compounds was investigated in  $1 \text{ mol L}^{-1} \text{ H}_2\text{SO}_4$  medium using PP and EIS. The results indicated that the order of corrosion inhibiting efficacy for the tested inhibitors in  $1 \text{ mol L}^{-1} \text{ H}_2\text{SO}_4$  solution was  $\text{Inh-3} > \text{Inh-2} > \text{Inh-1}$ . The PP results

Received: August 7, 2023

Accepted: September 27, 2023

Published: October 12, 2023



## Scheme 1. Synthesis of SBs

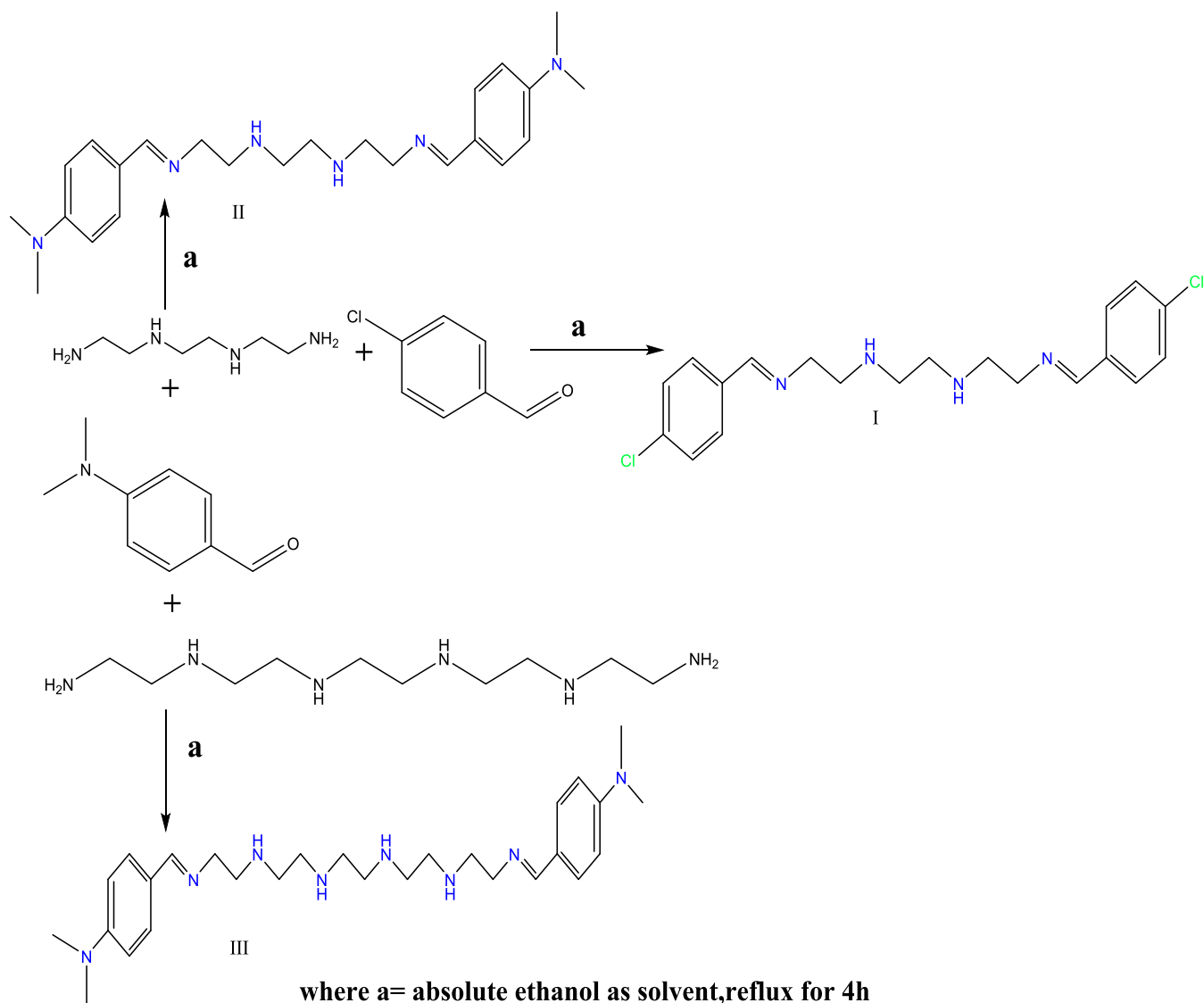


Table 1. Elemental Analysis for I, II, and III

cpd.	C%		H%		N%		Cl %		yield (%)
	cal.	obs.	cal.	obs.	cal.	obs.	cal.	obs.	
I	61.38	60.54	6.18	6.92	14.32	13.82	18.12	19.08	87
II	70.55	71.83	8.88	9.01	20.57	21.67			93
III	67.98	67.01	9.37	8.58	32.65	31.55			96

revealed that these molecules acted as efficient corrosion inhibitors with a mixed inhibition type.

In another study, Upadhyay et al.<sup>24</sup> reported on the corrosion inhibition potential of certain 4-aminoantipyrine-based Schiff bases, which contained OCH<sub>3</sub>, OH, and NMe<sub>2</sub> substituents in 1 N HCl aqueous medium using electrochemical methods. The findings revealed that the compound with a methoxy group exhibited higher efficiency compared to the others.

In their study, EL Basiony et al.<sup>14</sup> synthesized two unsymmetrical Schiff bases, namely, *N*-(2-((*Z*)-2-(benzylideneamino)ethylamino)ethyl)-3,4,5-trihydroxybenzamide (referred to as Bz) and *N*-(2-((*Z*)-2-(3-methoxy-4-hydroxybenzylideneamino)ethylamino)ethyl)-3,4,5-trihydroxybenzamide

Table 2. Infrared Spectra of (I–III) (Wavenumber cm<sup>-1</sup>)

cpd.	CH-H <sub>2</sub> O	C–H aromatic	C–H aliphatic	C=C aromatic	C=N
I	3420	3050	2935–2818	1164	1644
II	3385	3120	2892–2806	1178	1630
III	3406	3001	2822	1166	1660

(referred to as VA). The purpose was to investigate their inhibitory effect as acid corrosion inhibitors for mild steel (MS) in a 0.5 M HCl solution using the electrochemical method. The results indicated that both compounds (Bz and VA) acted as mixed-type inhibitors. Furthermore, the inhibition efficiency of VA was found to be superior to that

Table 3. Chemical Shifts ( $\delta$ ) of Compounds I, II, and III

cpd.	chemical shifts of different types of protons ( $\delta$ ppm)										
	a	b	c	d	e	f	g	i	h	j	k
I	8.20 (s)	7.66 (d)	7.48 (d)	3.60 (t)	3.30 (t)	2.6 (q)	1.05 (m)				
II	8.03 (s)	7.50 (d)	6.65 (d)	3.67 (t)	3.45 (t)	2.94 (q)	1.80 (m)	2.95 (s)			
III	8.13 (s)	7.80 (d)	6.78 (d)	3.96 (t)	3.73 (t)	3.04 (q)	2.93 (m)	2.87 (m)	2.88 (m)	1.88 (m)	2.9 (s)

s = singlet, d = doublet, t = triplet, q = quartet, and m = multiplet.

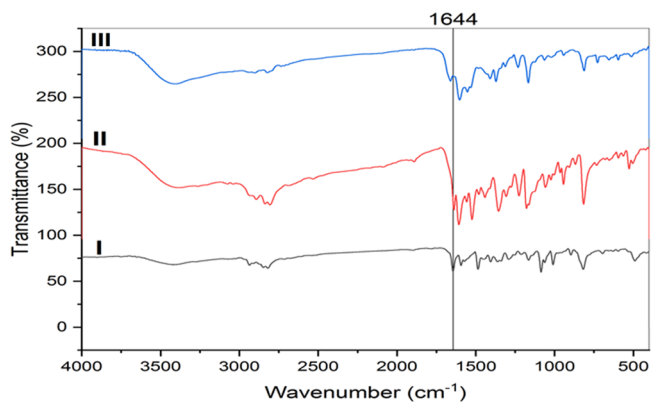


Figure 1. IR for prepared compounds I–III.  $^1\text{H}$  NMR: Data for  $^1\text{H}$  NMR for prepared SB derivatives shown in Table 3 and Figures 2–4

of Bz. The study aimed to examine the impact of the spacer in the Schiff base compound as an anticorrosion method.

## EXPERIMENT PART

**Materials.** The carbon steel specimen employed in this research possesses the following chemical composition (expressed in wt %): 0.093 (C), 0.014 (P), 0.011 (Si), 0.853 (Mn), 0.025 (Cr), 0.012 (Cu), 0.032 (Al), 0.013 (Ni), with the remaining being iron (Fe). The azo methane compounds used in the experiment were prepared using chemicals of pure

analytical grade, sourced from reputable suppliers, such as Sigma and Merck Company. The corrosive acidic solution utilized in the study is a 1 M HCl solution, prepared from high-quality HCl (37%, AR grade) obtained from Merck, and mixed with deionized water. The corrosion inhibitors were tested at concentrations ranging from 50 to 250 ppm.

**Synthesis of Schiff Bases I, II, and III.** Three SBs were prepared from the reaction A solution of amine derivatives  $\text{N1,N1}'$ -(ethane-1,2-diyl)bis(ethane-1,2-diamine) (I and II) or  $\text{N1,N1}'$ -(ethane-1,2-diyl)bis( $\text{N2}$ -(2-aminoethyl)ethane-1,2-diamine) (III) (0.005 mmol) in the ethanol solvent (15 mL). 4-Chlorobenzaldehyde (I) or 4-(dimethylamino)benzaldehyde (II and III) (0.01 mmol) was added drop by drop to a refluxing solution containing amino derivatives in absolute ethanol (20 mL). The solution obtained was gently refluxed under magnetic stirring for a period of 4 h, during which a change in color was noted. Subsequently, the solution was concentrated under vacuum, reducing its volume to one-third. Diethyl ether was introduced into the solution, and the mixture was cooled at 0 °C for 24 h. As a result, yellow crystals began to form, which were then filtered and dried under vacuum. However, it is important to note that at room temperature, these crystals proved to be unstable, and a yellow oil was obtained instead (see Scheme 1).

**Characterization of Anticorrosion.** The synthesized Schiff base compounds were characterized by elemental analysis with a PerkinElmer 240C elemental analyzer. The infrared spectrum

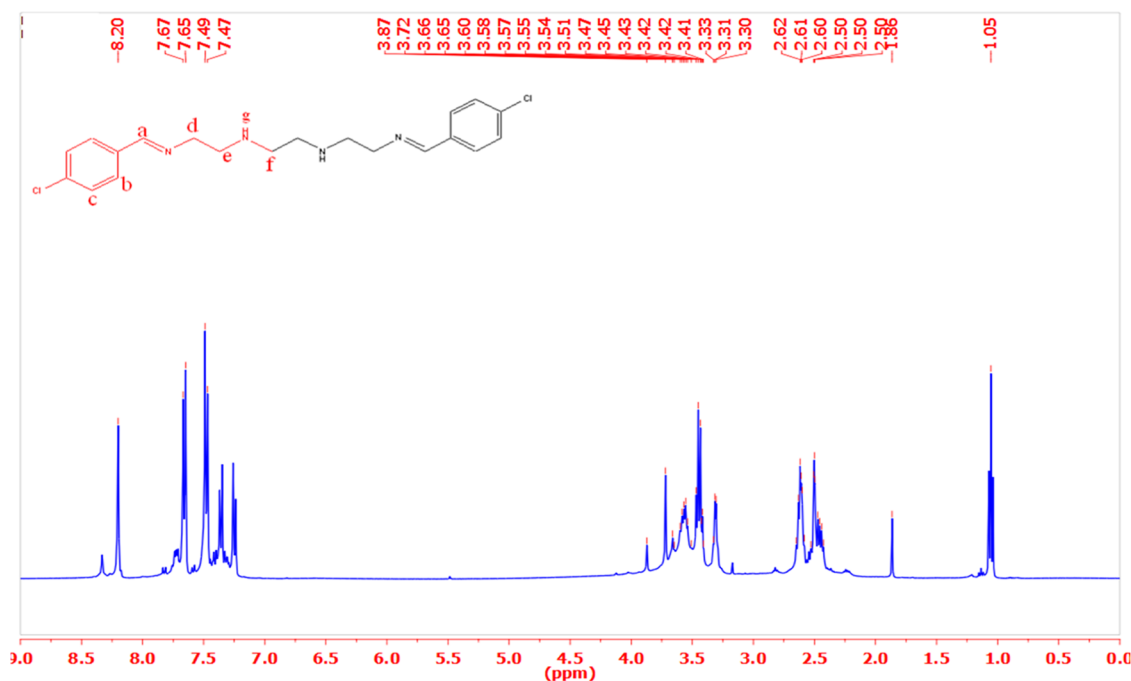


Figure 2.  $^1\text{H}$  NMR for the prepared compound I.

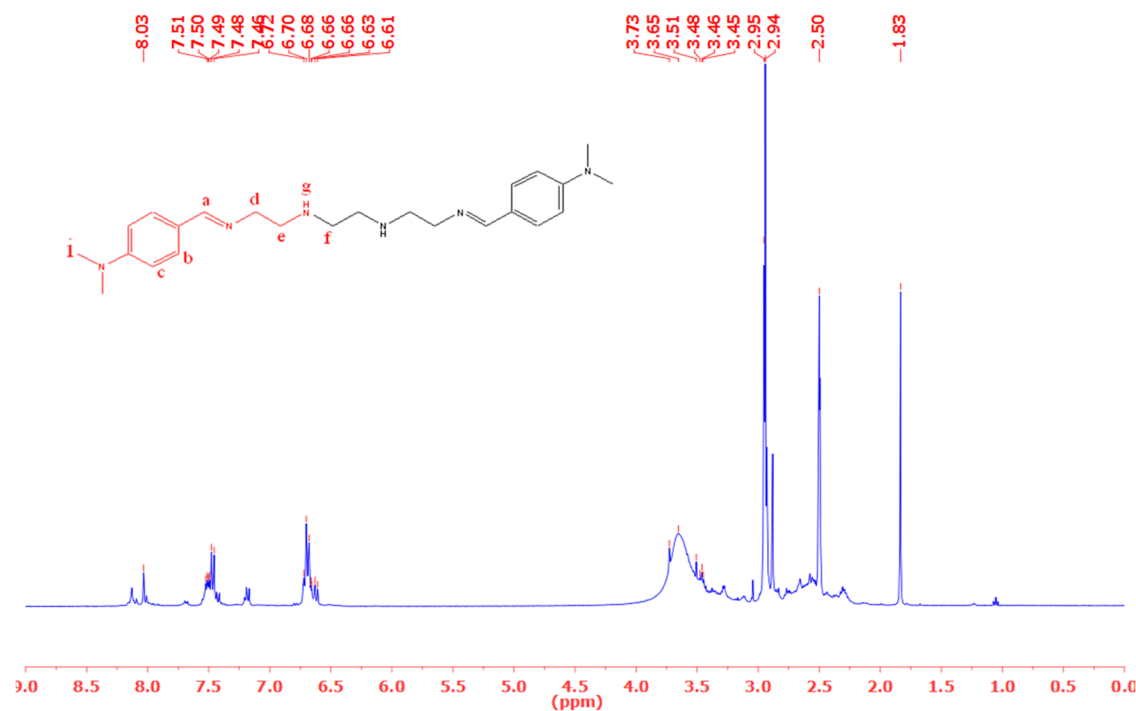


Figure 3.  $^1\text{H}$  NMR spectra for the prepared compound II.

Table 4. Electrochemical Kinetic Parameters Obtained by the EFM Technique of Steel in 1.0 M HCl in the Absence and Presence of Different Concentrations of I, II, and III at 25 °C

cpd.	conc (ppm).	$I_{\text{corr}}$ ( $\mu\text{A cm}^{-2}$ )	$\beta_a$ (mV dec $^{-1}$ )	$\beta_c$ (mV dec $^{-1}$ )	CF-2	CF-3	$k$ (mpy)	$\theta$	$\hat{\eta}_{\text{EFM}}$ %
blank	0.00	187.9	84.3	96.8	2.231	3.102	85.84		
I	50	63.85	73.32	81.71	3.018	2.217	29.18	0.6601	66.02
	100	62.82	43.56	50.17	2.886	2.49	28.71	0.6656	66.56
	150	51.72	79.67	91.16	1.828	3.376	23.63	0.7247	72.47
	200	49.83	38.58	45.82	1.979	1.426	22.77	0.7348	73.48
	250	41.2	44.61	58.7	1.889	2.49	18.83	0.7807	78.07
II	50	68.74	54.74	59.82	3.01	2.817	31.41	0.6341	63.41
	100	63.76	55.2	60.31	3.12	2.464	29.13	0.6606	66.06
	150	43.06	49.30	54.82	2.89	2.606	19.68	0.7708	77.08
	200	20.84	29.11	32.02	1.221	2.78	9.523	0.8891	88.91
	250	20.69	25.65	26.58	1.72	2.75	9.452	0.8899	88.99
III	50	63.27	56.17	63.86	1.041	3.341	28.91	0.6632	66.32
	100	57.55	41.67	48.30	1.601	2.958	26.30	0.6937	69.37
	150	22.71	47.47	52.95	1.69	2.763	10.38	0.8791	87.91
	200	22.65	55.93	62.44	1.58	3.802	10.35	0.8794	87.94
	250	11.77	24.43	25.63	1.21	2.13	5.377	0.9373	93.73

was analyzed by using an FTIR Spectrometer Model Type Mattson Benchtop 961 at wavenumbers 400–4000  $\text{cm}^{-1}$  and  $^1\text{H}$  NMR spectroscopy was conducted with a BRUKER instrument operating at 400.19 MHz using a 5 mm broad band inverse Z-gradient probe in DMSO  $d_6$  solvent.

**Electrochemical Measurements.** Potentiodynamic polarization measurements were performed using a Gamry Potentiostat Reference 3000 model number and 992-00051 corrosion software. For the electrochemical experiments, a conventional three-electrode cell configuration was used, consisting of a platinum wire counter electrode, a saturated calomel electrode as the reference electrode, and a carbon steel working electrode. The working electrode was meticulously machined into a cylindrical shape with dimensions of 2 cm in length and 1 cm in cross-sectional diameter, following the

procedure described in reference 25. A HCl solution (1 M) was prepared with distilled water from 37% HCl. The concentration range of the synthesized inhibitor was from 50 to 250 ppm.

The working electrode was immersed in 50 mL of the aggressive solution (1 M HCl) under varying concentrations of each compound, ranging from 50 to 250 ppm, all conducted at a controlled temperature of 25 °C.

EIS was performed after allowing the working electrode to immerse in the aggressive solution for a duration of 1 h while maintaining the open-circuit potential (OCP) condition. A small alternating voltage perturbation of 10 mV (peak to peak) was applied to the cell over a frequency range spanning from 100 kHz to 20 mHz at the same temperature of 25 °C. This technique provided insights into the electrical properties and impedance responses of the system. Furthermore, part per

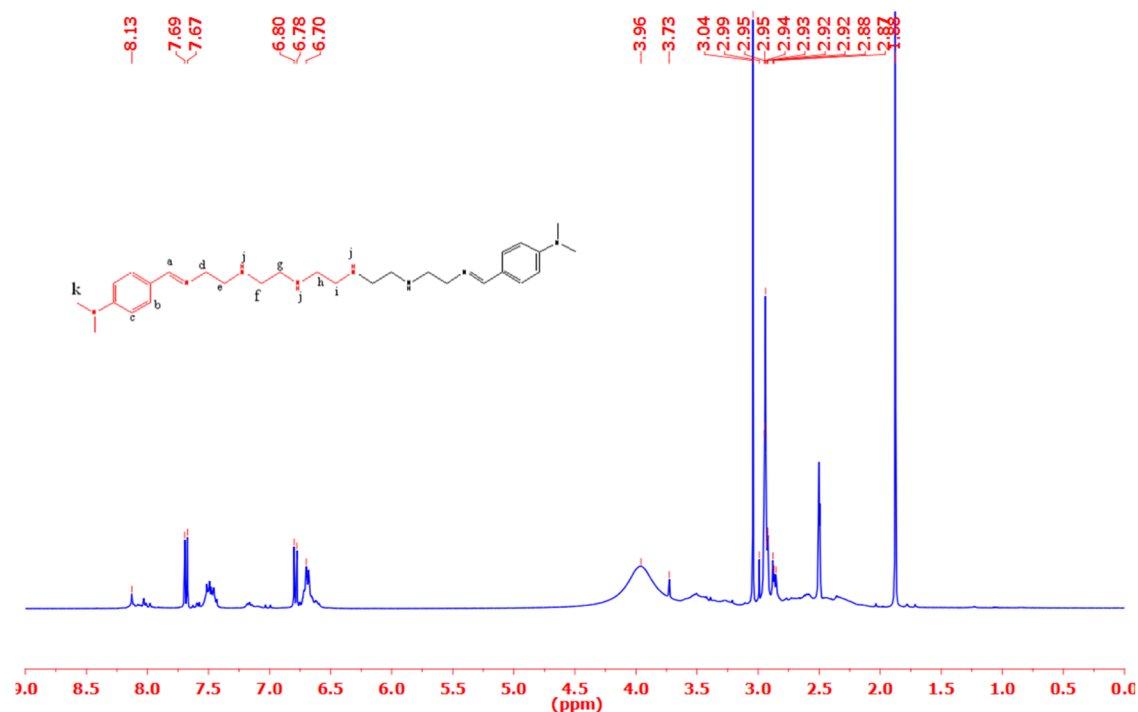


Figure 4.  $^1\text{H}$  NMR spectra for the prepared compound III.

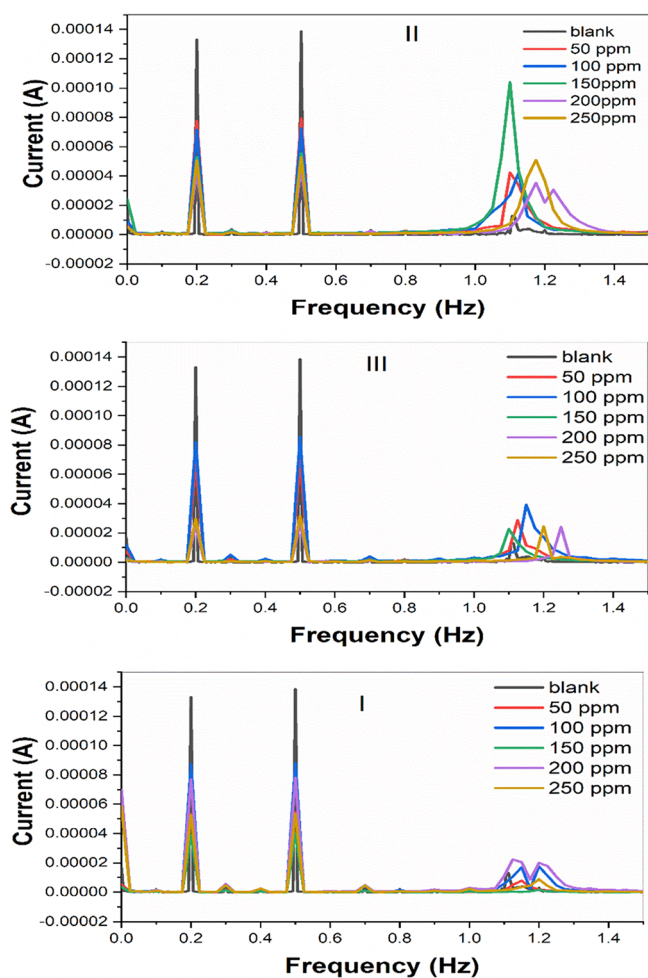


Figure 5. EFM for inhibitors I, II, and III in 1 M HCl without and with inhibitor and with different concentrations.

million measurements were conducted at a scan rate of  $0.5 \text{ mV s}^{-1}$  to investigate the electrochemical response and behavior of the system under study. For a more comprehensive analysis, EFM was also employed. With an AC amplitude of 10 mV, two different frequencies, namely, 2 and 5 Hz, were applied during the experiments, contributing valuable information on the kinetics and performance of the inhibitors in the aggressive environment.<sup>15,26–29</sup>

**Scanning Electron Microscope (SEM).** A scanning electron microscope (SEM) was used to examine the exterior surface morphology of the carbon steel surface when the inhibitors (I, II, and III) were present and absent. SEM was assessed using a ZEISS EVO 10.

**Theoretical Study for Inhibition (I–III).** The molecules under investigation were designed and subjected to geometric optimization using the DMol<sub>3</sub> calculation model available in Materials Studio v7.0.<sup>30</sup> The setup involved geometry optimization with fine quality and the LDA functional, considering all electrons in the core treatment and utilizing the DNP basis set.

The energies of the highest occupied molecular orbital ( $E_{\text{HOMO}}$ ) and the lowest unoccupied molecular orbital ( $E_{\text{LUMO}}$ ) were determined through calculations. From these energy values, the parameters  $I$ ,  $A$ ,  $\chi$ , and  $\eta$  were computed using equations previously established in the literature.<sup>31</sup>

## RESULTS AND DISCUSSION

**Characterization of Structures for I–III. Elemental Analysis.** The data presented in Table 1 demonstrate that the calculated percentages for each element closely match the observed values.

**FTIR Spectroscopy.** Table 2 provides a comprehensive summary of infrared (IR) spectroscopy data for three distinct compounds or chemical groups. For compound I, the  $3420 \text{ cm}^{-1}$  frequency signifies the presence of hydrogen atoms bonded to oxygen, indicating the presence of water.<sup>32–34</sup>

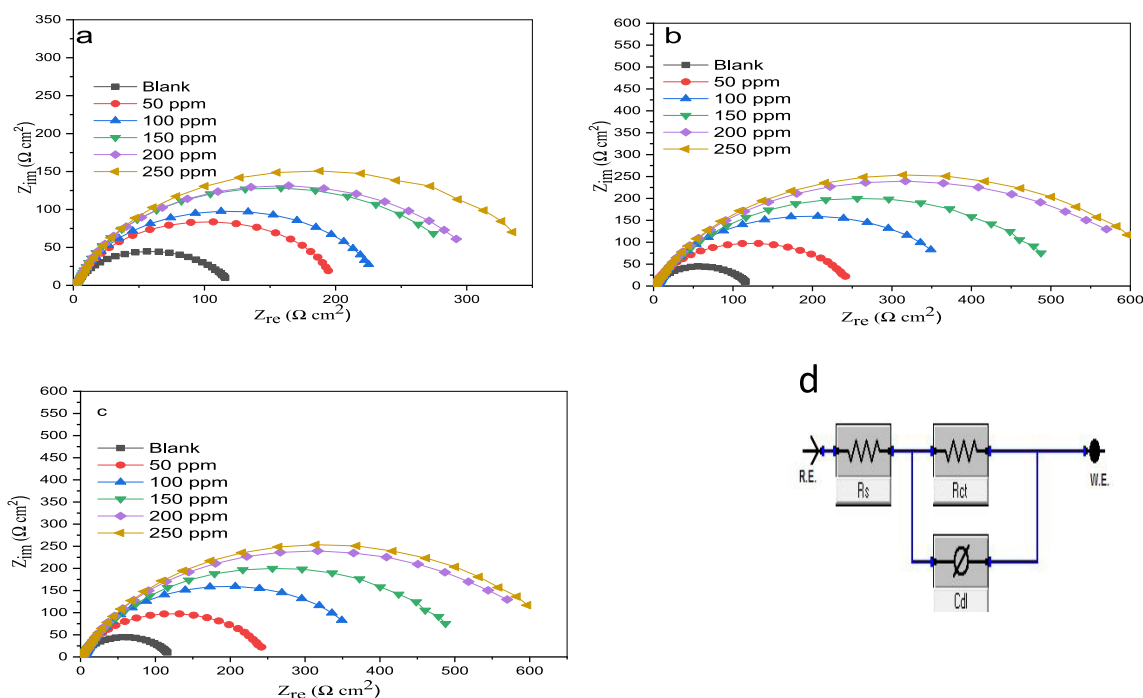


**Figure 6.** Nyquist diagrams for carbon steel in 1 M HCl with different concentrations of I (a), Nyquist diagrams for carbon steel in 1 M HCl with different concentrations of II (b), Nyquist diagrams for carbon steel in 1 M HCl with different concentrations of III (c), and equivalent circuit model for the impedance analysis (d).

Additionally, a frequency of  $3050\text{ cm}^{-1}$  suggests the presence of hydrogen atoms within aromatic (ring-like) hydrocarbon structures, while the range of  $2935\text{--}2818\text{ cm}^{-1}$  indicates absorption linked to hydrogen atoms in aliphatic (non-aromatic) hydrocarbon structures. At  $1164\text{ cm}^{-1}$ , evidence emerges of carbon–carbon double bonds within aromatic compounds, and a peak at  $1644\text{ cm}^{-1}$  implies the presence of carbon–nitrogen double bonds. For compound II, similar characteristics are observed, such as the  $3420\text{ cm}^{-1}$  absorption, indicating hydrogen atoms bonded to oxygen, and the  $3050\text{ cm}^{-1}$  absorption, indicating hydrogen atoms in aromatic hydrocarbon structures. The range of  $2892\text{--}2806\text{ cm}^{-1}$  reveals the absorption associated with hydrogen atoms in aliphatic hydrocarbon structures, and an absorption peak at  $1178\text{ cm}^{-1}$  indicates carbon–carbon double bonds within aromatic compounds, with a peak at  $1630\text{ cm}^{-1}$ , suggesting carbon–nitrogen double bonds (Table 3). In the case of compound III, the  $3406\text{ cm}^{-1}$  absorption suggests hydrogen atoms bonded to oxygen, while the  $3001\text{ cm}^{-1}$  frequency hints at hydrogen atoms in aromatic hydrocarbon structures. Furthermore, the  $2822\text{ cm}^{-1}$  absorption corresponds to hydrogen atoms in aliphatic hydrocarbon structures. A frequency of  $1166\text{ cm}^{-1}$  implies the presence of carbon–carbon double bonds within aromatic compounds, and a peak at  $1660\text{ cm}^{-1}$  suggests carbon–nitrogen double bonds. These distinctive IR absorption frequencies offer valuable insights into the molecular compositions and functional groups present in each compound or chemical group (Figures 1 and 2).

- Compound I exhibits a singlet (s) at  $\delta = 8.20\text{ ppm}$ , indicating a set of equivalent protons in a specific chemical environment. The other signals in this compound are doublets (d), triplets (t), quartets (q), and multiplets (m), each with their own  $\delta$  ppm values, suggesting the presence of distinct proton environments within the molecule.

- Compound II also displays a singlet (s) at  $\delta = 8.03\text{ ppm}$ , and, like compound I, features doublets (d), triplets (t), quartets (q), and multiplets (m) with varying  $\delta$  ppm values. These different shifts represent different proton environments within the compound.
- Compound III, like the previous compounds, has a singlet (s) at  $\delta = 8.13\text{ ppm}$ . Additionally, it exhibits doublets (d), triplets (t), quartets (q), and multiples (m) with their respective  $\delta$  ppm values, demonstrating diverse proton environments. Overall, the  $^1\text{H}$  NMR spectrum can provide valuable information about the identity and structure of compounds (Figure 3).

**Evaluation of the Inhibitor as Anticorrosion.** EFM technique has been used to obtain Tafel slopes as well as corrosion current densities for carbon steel immersed in 1 M HCl with and without SB, and the data for inhibitor III are tabulated in Table 4 and shown in Figures 4 and 5.<sup>35,36</sup> The following equations present the parameter obtained from the EFM technique for all SB derivatives with different concentrations.

$$i_{\text{corr}} = \frac{i_{\omega}^2}{\sqrt{482i_{\omega}i_{3\omega} - i_{2\omega}^2}} \quad (1)$$

$$\beta_a = \frac{i_{\omega}U_o}{2i_{2\omega} + 2\sqrt{3}\sqrt{2i_{3\omega}i_{\omega} - i_{2\omega}^2}} \quad (2)$$

$$\beta_c = \frac{i_{\omega}U_o}{2\sqrt{3}\sqrt{2i_{3\omega}i_{\omega} - i_{2\omega}^2} - 2i_{2\omega}} \quad (3)$$

$$\text{causality factor}(2) = \frac{i_{\omega 2 \pm \omega 1}}{i_{2\omega 1}} = 2.0 \quad (4)$$

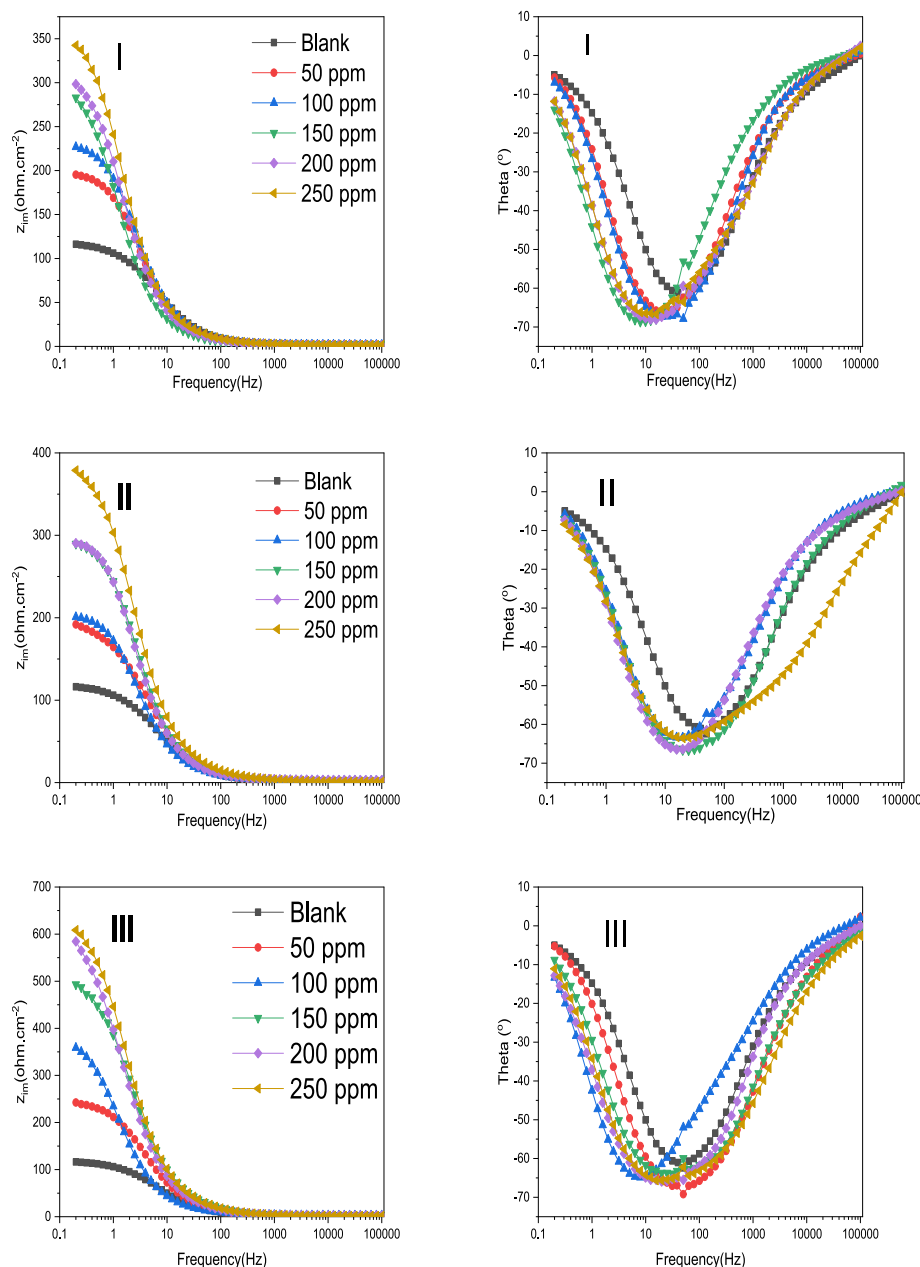


**Figure 7.** Bode plots of carbon steel in 1.0 M HCl with an inhibitor (I–III).

$$\text{causality factor}(3) = \frac{i_{2\omega 2 \pm \omega 1}}{i_{3\omega 1}} = 3.0 \quad (5)$$

where  $[i]$  denotes the current density at an instant, measured during the frequency  $[\omega]$ , while  $[U_o]$  refers to the amplitude of the sine wave distortion.

Furthermore, the corrosion current densities acquired from the experiments were employed to determine the inhibition efficiency. This was achieved by substituting these values for the following equation

$$\eta_{\text{EFM}} \% = \left( 1 - \frac{i_{\text{corr}}}{i_{\text{corr}}^0} \right) \times 100 \quad (6)$$

The results clearly indicate a decrease in the corrosion current densities for carbon steel as the inhibitor concentration increases. Notably, inhibitor III showed an impressive

inhibition percentage of 93% at a high concentration of 250 ppm. Figures 6 and 7 display the Nyquist plots obtained at OCP and 25 °C, both with and without the compounds, in 1 M HCl. The corresponding results are presented in Table 5, utilizing the equivalent circuit shown in Figure 6d. As the concentration of SBs increases for all derivatives, a notable increase in the diameter of the semicircle is observed. Additionally, the capacitive loop of the Bode plot becomes more pronounced with increasing SB concentrations, indicating a lower corrosion rate in the presence of SB.<sup>37</sup>

Table 6 provides a summary of the changes observed in the solution resistance ( $R_s$ ), charge transfer resistance ( $R_{ct}$ ), and double-layer capacitance ( $C_{dl}$ ). It is evident that the  $R_{ct}$  values increase as the inhibitor concentration increases, while the  $C_{dl}$  values decrease. The reduction in  $C_{dl}$  is attributed to a decrease in the local dielectric constant or an increase in the electrical double layer's thickness, indicating the adsorption of inhibitors

**Table 5. EIS Parameters of Steel in 1.0 M HCl in the Absence and Presence of Different Concentrations of I, II, and III at 25 °C**

cpd.	conc (ppm).	$R_s$ ( $R_u$ ) ( $\Omega$ cm <sup>2</sup> )	$R_{ct}$ ( $R_p$ ) ( $\Omega$ cm <sup>2</sup> )	$Y_o$ ( $\mu$ $\Omega^{-1}$ s <sup>n</sup> cm <sup>-2</sup> ) $\times 10^{-2}$	$n$	$X^2 \times 10^{-3}$	$\theta$	$\eta_z$ %
blank	0.00	1.68	119.8	612	0.805	1.38	-	-
I	50	9.96	200.8	542	0.808	3.28	0.4033	40.33
	100	2.503	219.6	671	0.821	2.48	0.4544	45.44
	150	2.03	315.3	457	0.832	1.88	0.6200	62.00
	200	3.157	320.1	492	0.839	3.66	0.6257	62.57
	250	1.064	456	531	0.742	6.78	0.7372	73.72
II	50	2.04	208.6	603	0.84	2.13	0.4257	42.57
	100	1.85	241.8	556	0.851	1.23	0.5045	50.45
	150	2.437	326.1	909	0.848	3.95	0.6326	63.26
	200	1.356	352.8	804	0.808	5.04	0.6604	66.04
	250	2.407	526.2	788	0.774	8.35	0.7737	77.37
III	50	1.23	254.2	411	0.825	1.57	0.5287	52.87
	100	2.698	460.2	860	0.772	8.2	0.7396	73.96
	150	2.01	553.7	354	0.785	1.56	0.7836	78.36
	200	2.37	656.1	387	0.807	8.43	0.8174	81.74
	250	1.57	711.9	358	0.708	2.59	0.8317	83.17

**Table 6. Corrosion Parameters Obtained from Potentiodynamic Polarization Measurements of Steel in 1.0 M HCl in the Absence and Presence of Different Concentrations of I, II, and III at 25 °C**

cpd.	conc (ppm).	-Eco. mV vs SCE	$I_{co}$ ( $\mu$ Acm <sup>-2</sup> )	$\beta_a$ (mV dec <sup>-1</sup> )	$\beta_c$ (mV dec <sup>-1</sup> )	$X^2$	$k$ (mpy)	$\theta$	$\eta_z$ %
blank	0.00	396	320	142.1	224	33.79	146.3	-	-
I	50	415	171	143	188	36.44	77.98	0.4656	46.56
	100	413	159	134	192	24.32	72.79	0.5031	50.31
	150	401	139	133	199	17.04	63.69	0.5656	56.56
	200	415	120	139	201	47.44	54.78	0.6250	62.5
	250	411	70.7	101	160	33.8	32.29	0.7791	77.91
II	50	411	138	114	171	28.28	63.20	0.5688	56.88
	100	394	114	107	194	48.42	51.94	0.6438	64.3
	150	423	87.3	128	213	54.27	39.91	0.7272	72.72
	200	411	65.9	111	221	71.23	30.10	0.7941	79.41
	250	419	60.4	122	194	66.25	27.61	0.8113	81.13
III	50	392	107	111	158	15.7	48.70	0.6656	66.56
	100	391	86.9	108	157	23.01	39.72	0.7284	72.84
	150	381	77.7	102	175	42.4	35.50	0.7572	75.72
	200	379	61.9	98	157	29.63	28.28	0.8065	80.65
	250	376	46.8	87	162	40.95	21.38	0.8538	85.38

at the metal/solution interface. The inhibition efficiency was determined using the following equation<sup>38,39</sup>

$$\theta = [(R_{oct} - R_{ct})/R_{oct}] \quad (7)$$

$$\eta_z\% = [(R_{oct} - R_{ct})/R_{oct}] \times 100 \quad (8)$$

where  $R_{ct}$  represents the charge transfer resistance in the presence of inhibitors, while  $R_{oct}$  signifies the charge transfer resistance without the inhibitors. The inhibition efficiency exhibits a positive correlation with the inhibitor concentration, reaching a peak value of 83% for inhibitor III.

Figure 8 illustrates PP curves for carbon steel in 1 M HCl, both in the presence and absence of inhibitors I, II, and III at 25 °C. The values of various electrochemical parameters, including corrosion current density ( $I_{corr}$ ), corrosion potential ( $E_{corr}$ ), cathodic and anodic Tafel slopes ( $\beta_c$  and  $\beta_a$ ), as well as inhibition efficiency, are summarized in Table 5.

The figures provide clear evidence that the synthesized inhibitors effectively reduce the corrosion rate, leading to a noticeable shift in both the anodic and cathodic branches of the Tafel plots toward lower current density values across all

concentrations. This suggests that these compounds effectively inhibit both hydrogen evolution and carbon steel dissolution reactions. The highest inhibition efficiency, reaching 83%, was observed for compound III at a concentration of 250 ppm. The inhibition efficiency (IE) and degree of surface coverage ( $\theta$ ) were determined using the following equations<sup>40</sup>

$$\theta = [(I_{0corr} - I_{corr})/I_{0corr}] \quad (9)$$

$$IE\% = [(I_{0corr} - I_{corr})/I_{0corr}] \times 100 \quad (10)$$

where  $I_{corr}$  and  $I_{0corr}$  denote the inhibited and uninhibited corrosion current densities, respectively.

Based on the results obtained from electrochemical frequency modulation (EFM), electrochemical impedance spectroscopy (EIS), and polarization (PP) experiments, it is evident that the Schiff base compounds (I, II, III) possess a remarkable capacity to efficiently inhibit the corrosion of steel in acidic solutions. This inhibitory effect can be attributed to the presence of electronegative atoms, such as N, unsaturated double bonds, azomethine linkage, and planar conjugated systems within their aromatic rings.<sup>41-44</sup>

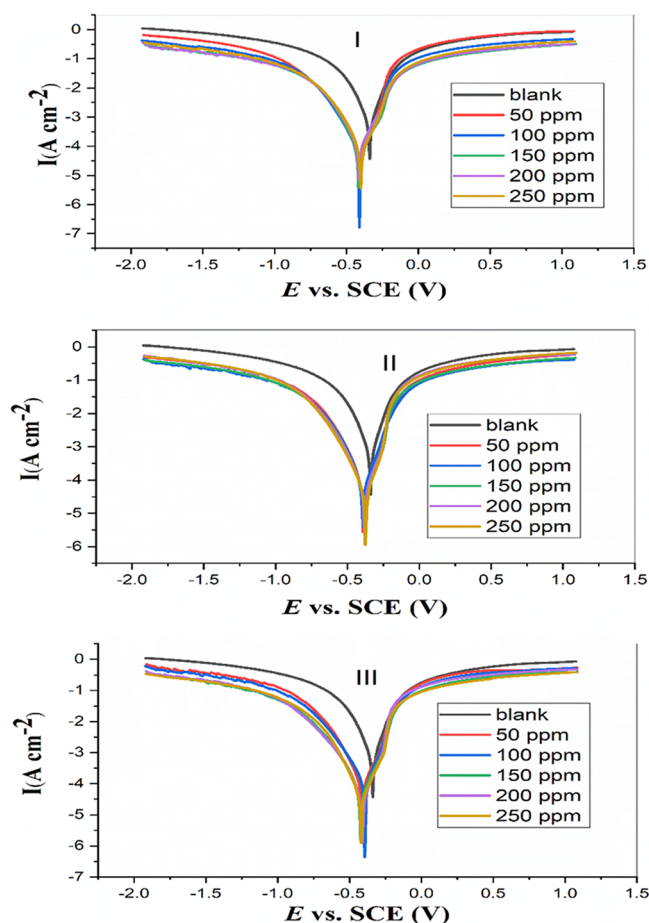


**Figure 8.** PP curves for the corrosion of carbon steel in 1 M HCl in the absence and presence of different concentrations of I, II, and III.

**Adsorption Isotherm.** The adsorption isotherm serves as a valuable means of characterizing the types, locations, and frequencies of interactions between a metal surface and an inhibitor. It establishes the connection between the surface coverage ( $\theta$ ) of the metal and the concentration ( $C$ ) of the inhibitor in a corrosive environment. In this study, we utilized the Langmuir adsorption isotherm, described by the equation, as it more accurately depicts the adsorption behavior of SB on mild steel surfaces.<sup>14,45,46</sup> The data collected from EFM were utilized in the subsequent application of the following equation

$$\frac{c}{\theta} = \frac{1}{k} + c \quad (11)$$

In Figure 9 and Table 7, the obtained values are for  $K_{\text{ads}}$ , which represents the equilibrium constant of the inhibitor adsorption process. These higher  $K_{\text{ads}}$  values indicate a more robust adsorption of the azo compounds on the surface of carbon steel.<sup>47,48</sup> The calculation of the free energy of adsorption  $\Delta G_{\text{ads}}^0$  was performed using the following equation<sup>49</sup>

$$\Delta G_{\text{ads}}^0 = -RT \ln(10^6 K_{\text{ads}}) \quad (12)$$

The factor  $10^6$  corresponds to the concentration of water molecules in the solution (measured in mol/L), and  $R$  denotes the universal gas constant with a value of  $8.314 \text{ J K}^{-1} \text{ mol}^{-1}$ . The  $\Delta G_{\text{ads}}^0$  values for I, II, and III are determined as  $-58.57$ ,  $-54.88$ , and  $-55.67 \text{ kJ/mol}$ , respectively.

The  $\Delta G_{\text{ads}}^0$  value determines the type of adsorption process as follows: (i) If  $\Delta G_{\text{ads}}^0$  is less negative than  $-20 \text{ kJ/mol}$ , the

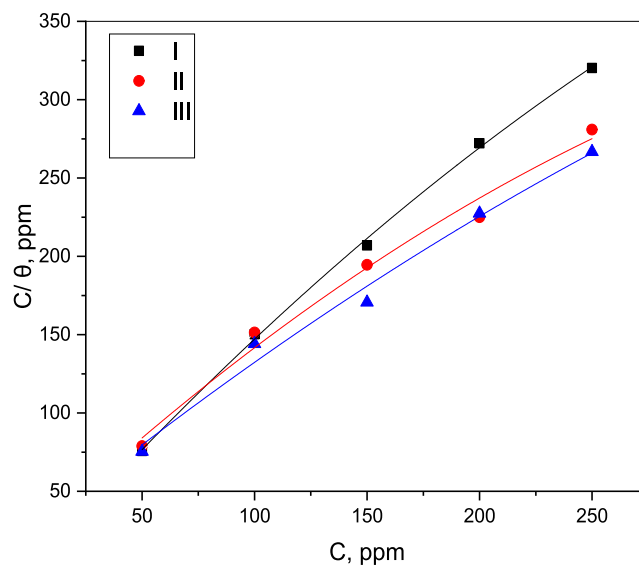


**Figure 9.** Langmuir adsorption isotherms for SB, obtained from EFM data.

**Table 7.** Langmuir Adsorption Parameters for the Adsorption of SB on Carbon Steel at 25 °C

inhibitor	$R^2$	$K_{\text{ads}}$ ( $\text{ppm}^{-1}$ )	$\Delta G_{\text{ads}}^0$
I	0.9936	0.0459	$-58.57$
II	0.9737	0.0234	$-54.88$
III	0.9802	0.0269	$-55.67$

adsorption is considered physical (referred to as physisorption), which occurs through electrostatic interactions. (ii) If  $\Delta G_{\text{ads}}^0$  is more negative than  $-40 \text{ kJ/mol}$ , the adsorption is classified as chemical (known as chemisorption), where coordinate bonds are formed via electron transfer from inhibitor molecules to the metal surface. (iii) When  $\Delta G_{\text{ads}}^0$  falls between  $-20$  and  $-40 \text{ kJ/mol}$ , the types of adsorption, physisorption, and chemisorption are involved.<sup>50–53</sup> For SB, the  $\Delta G_{\text{ads}}^0$  value is more than  $-40 \text{ kJ mol}^{-1}$ , which indicates the occurrence of chemisorption processes.

**Surface Morphological Study.** The SEM image of CS submerged in 1.0 M HCl at room temperature 25 °C for 6 h is shown in Figure 10a, which represents the micrograph of a blank sample in the absence of inhibitors; the steel surface had a hard corroded appearance with significant surface deterioration. In comparison, in the micrographs of the specimen CS samples in the presence of 250 ppm of the inhibitors into the acid solutions I, II, and III (Figure 10b–d), respectively, the corrosion rate of metal is significantly reduced, and the steel surface was smooth; the corroded areas were clearly lessened that indicates the surface protection because of the adsorption of I, II, and III inhibitors onto the steel surface.

**Quantum Chemical Calculations.** Molecular orbital density, HOMO, and LUMO are presented in Figures 11, 12, and 13, respectively, while the quantum chemical parameter is shown in Table 8. Electron density of HOMO indicates that most atoms tend to donate electrons to lower-energy empty molecular orbitals in the order III > II > I.

In addition, in this molecule, a feedback bond can be formed depending on  $E_{\text{LUMO}}$ , suggesting that electrons from the d orbital of the metal can be easily accepted.<sup>54</sup> The electron densities of HOMO are localized on and around the azo

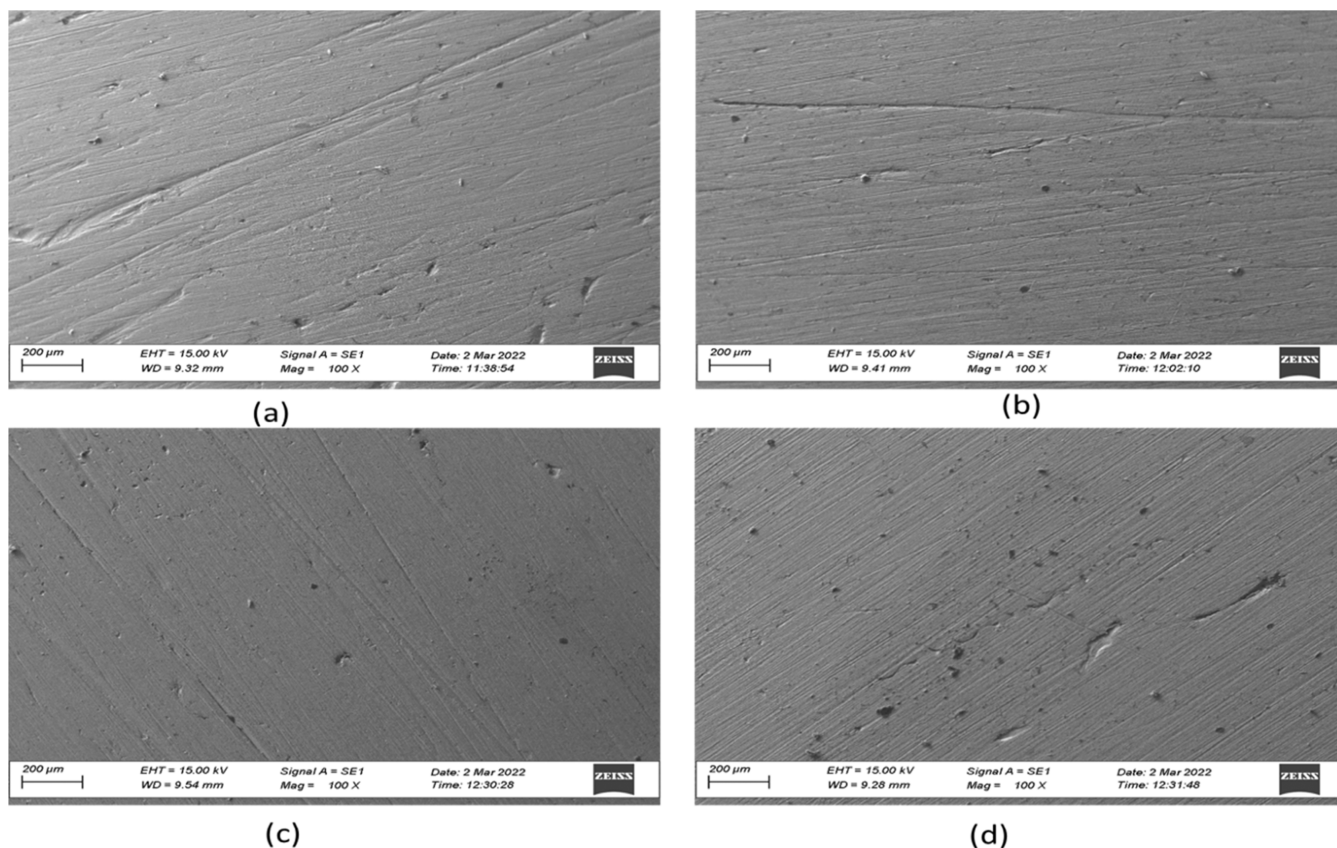


**Figure 10.** SEM images for the carbon steel surface in the solutions after 6 h immersed at room temperature: (a) 1.0 M HCl, (b) in the existence of 250 ppm of I, (c) in the existence of 250 ppm of II, and (D) in the existence of 250 ppm of III.

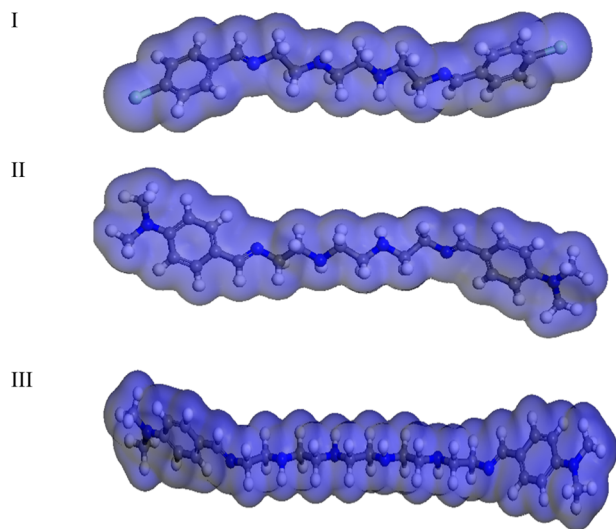


**Figure 11.** Electron densities for I–III.

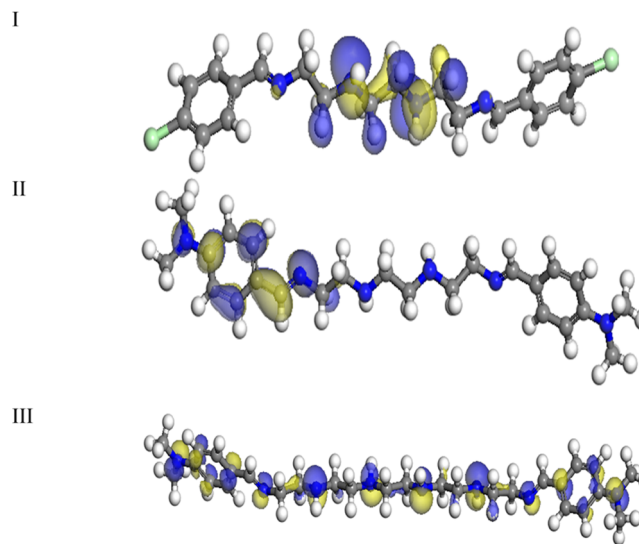


**Figure 12.** HOMO for I–III.

methane group for the I, II, and III molecules. It is observed that the side chains (Cl and  $N(\text{CH}_3)_2$ ) affect the electronic density distribution of the HOMO of the studied compounds. In addition to the spacer in compound III more than I and II, this led to an increase in the surface area covered by compound III and agreed with the Langmuir adsorption data.

Table 9 compares one of the inhibitors we investigated with those from the literature that are comparable in terms of chemistry and active function groups.<sup>16,55,56</sup>

## CONCLUSIONS

In conclusion, the novel Schiff base compounds I, II, and III were successfully synthesized and characterized using elemental analysis, FTIR spectroscopy, and  $^1\text{H}$  NMR spectroscopy. These compounds were investigated as potential anticorrosion agents for carbon steel in acidic environments. The electrochemical experiments, including EFM, EIS, and PP measurements, revealed that all three compounds effectively

Table 8. Chemical Parameter for Compounds I–III

chemical parameter			I	II	III
high occupied molecular orbital (eV)	$E_{\text{HOMO}}$		−0.1652	−0.1655	−0.1679
low unoccupied molecular orbital (eV)	$E_{\text{LUMO}}$		−0.0554	−0.0576	−0.0905
energy gap (eV)	$\Delta E_{\text{Gap}}$	$E_{\text{LUMO}} - E_{\text{HOMO}}$	0.1098	0.1079	0.0774
ionization potential (eV)	$I$	$-E_{\text{HOMO}}$	0.1652	0.1655	0.1679
electron affinity (eV)	$A$	$-E_{\text{LUMO}}$	0.0554	0.0576	0.0905
absolute electronegativity	$X$	$(I + A)/2$	0.1103	0.1116	0.1292
global hardness (eV)	$\eta$	$(I - A)/2$	0.0549	0.039	0.0387
global softness (eV) <sup>−1</sup>	$S$	$1/\eta$	18.215	2.5.641	25.839
global electrophilicity index (eV)	$\omega$	$\mu^2/2\eta$ where	−0.0549	−0.039	−0.0387
back-donation energy (eV)	$\Delta E_{\text{Back-donation}}$	$\eta/4$	0.0137	0.0098	0.0097

Table 9. Comparison of the Inhibition Efficiency of Our Investigated Inhibitors with Other Inhibitors from the Literature

inhibitor	medium	metal	concentration	IE%, according To PP technique (%)	ref
( <i>E</i> )-2-(1-triazylideneethyl)pyridine	1 M HCl	mild steel	10 <sup>−3</sup> M	77.7	55
quinolinyl thiopropano hydrazone derivative	1 M HCl	mild steel	11.08 × 10 <sup>−4</sup> M	88.9	56
<i>N</i> -(benzo[ <i>d</i> ]thiazol-2-yl)-1-(thiophene-2-yl)methanimine	1 M H <sub>2</sub> SO <sub>4</sub>	steel	1 × 10 <sup>−3</sup>	95.6	16
<i>N</i> <sub>1</sub> , <i>N</i> ' <sub>1</sub> -(ethane-1,2-diyl)bis( <i>N</i> <sub>2</sub> '-((( <i>Z</i> )-4-dimethylamino)benzylidene)amino)methylethane-1,2-diamine)	1 M HCl	mild steel	250 ppm	85.38	this study

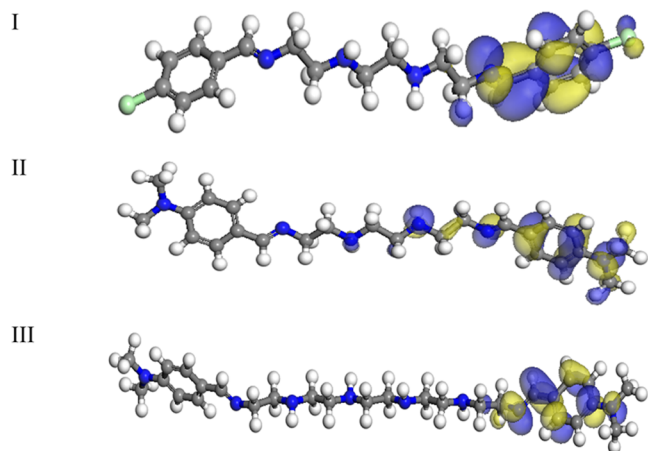


Figure 13. LUMO for I–III.

reduced the corrosion rate of carbon steel, with compound III showing the highest inhibition efficiency of 93% at a concentration of 250 ppm. The Langmuir adsorption isotherm provided insights into the adsorption behavior, and the calculated  $K_{\text{ads}}$  values indicated strong adsorption of the compounds on the carbon steel surface. The free energy of adsorption  $\Delta G_{\text{ads}}^0$  values suggested that the inhibition mechanism was chemisorption. Furthermore, quantum chemical calculations provided additional understanding of the electronic structure, and the analysis of HOMO and LUMO indicated that compound III had the highest surface coverage due to its specific molecular structure and spacer. This observation agreed well with the Langmuir adsorption data. Overall, the synthesized Schiff base compounds showed great promise as efficient anticorrosion agents for carbon steel in strongly acidic media, with compound III demonstrating the highest inhibitory performance. These findings open new possibilities for the design and development of effective corrosion inhibitors to protect carbon steel in various industrial applications.

## AUTHOR INFORMATION

### Corresponding Author

Ashraf M. Ashmawy – Chemistry Department, Faculty of Science (boys), Al-Azhar University, Nasr City 11884, Egypt; [orcid.org/0000-0002-8006-7605](https://orcid.org/0000-0002-8006-7605); Email: [ashraf\\_ashmawy2002@azhar.edu.eg](mailto:ashraf_ashmawy2002@azhar.edu.eg)

### Authors

Hamdy Khamees Thabet – Chemistry Department, Faculty of Arts and Science, Northern Border University, Rafha 91911, Saudi Arabia

Jwahr M. AlGhamdi – Department of Chemistry, College of Science, Imam Abdulrahman Bin Faisal University, 31451 Dammam, Saudi Arabia

Hoda A. Mohammed – Analysis and evaluation department, Egyptian Petroleum Research institute (EPRI), Cairo 11727, Egypt

Mahmoud A. M. Elsaid – Metallurgy Department, Nuclear Research Center (NRC), Egyptian Atomic Energy Authority (EAEA), Cairo 0202, Egypt

Complete contact information is available at: <https://pubs.acs.org/10.1021/acsomega.3c05790>

### Notes

The authors declare no competing financial interest.

## ACKNOWLEDGMENTS

The authors extend their appreciation to the Deputyship for Research & Innovation, Ministry of Education in Saudi Arabia for funding this research work through the project number “2023-0113”.

## REFERENCES

- (1) Kim, K.; Lim, H.; Sic Park, H.; Hong Kang, J.; Park, J.; Song, H. Effect of selected green corrosion inhibitors on SO<sub>2</sub> removal during carbon steel corrosion in aqueous solutions of ammonia and histidine. *J. Ind. Eng. Chem.* **2023**, *127*, 476–484.
- (2) Mohammed, H. K.; Jafar, S. A.; Humadi, J. I.; Sehgal, S.; Saxena, K. K.; Abdullah, G. H.; Saeed, L. I.; Salman, M. S.; Abdullah, W. S. Investigation of carbon steel corrosion rate in different acid

- environments. *Mater. Today: Proc.* **2023**, DOI: 10.1016/j.matpr.2023.03.792.
- (3) Basilio, E.; Marcelin, S.; Mingant, R.; Kittel, J.; Fregonese, M.; Ropital, F. The effect of chemical species on the electrochemical reactions and corrosion product layer of carbon steel in CO<sub>2</sub> aqueous environment: A review. *Mater. Corros.* **2021**, *72*, 1152–1167, DOI: 10.1002/maco.202012118.
- (4) Ibrahim, M. M.; Abdel Hameed, R.; Abu-Nawwas, A. A. H.; Mohamad, S. E. Schiff's Bases and Their Metal Complexes as Corrosion Inhibitors for Aluminum Alloys in Corrosive Media. *ChemInform* **2016**, 4721. DOI: 10.1002/chin.201612135
- (5) Sengupta, S.; Murmu, M.; Murmu, N. C.; Banerjee, P. Adsorption of redox-active Schiff bases and corrosion inhibiting property for mild steel in 1 molL<sup>-1</sup> H<sub>2</sub>SO<sub>4</sub>: Experimental analysis supported by ab initio DFT, DFTB and molecular dynamics simulation approach. *J. Mol. Liq.* **2021**, *326*, No. 115215.
- (6) Mook, W.; Aroua, M.; Issabayeva, G. Prospective applications of renewable energy based electrochemical systems in wastewater treatment: A review. *Renewable Sustainable Energy Rev.* **2014**, *38*, 36–46.
- (7) Grzesik, W. *Advanced Machining Processes of Metallic Materials: Theory, Modelling and Applications*; Elsevier, 2008.
- (8) Cui, F. Y.; Guo, L.; Zhang, S. T. Experimental and theoretical studies of 2-amino thiazole as an inhibitor for carbon steel corrosion in hydrochloric acid. *Mater. Corros.* **2014**, *65* (12), 1194–1201.
- (9) Behpour, M.; Ghoreishi, S.; Soltani, N.; Salavati-Niasari, M. The inhibitive effect of some bis-N, S-bidentate Schiff bases on corrosion behaviour of 304 stainless steel in hydrochloric acid solution. *Corros. Sci.* **2009**, *51* (5), 1073–1082.
- (10) Naderi, E.; Jafari, A.; Ehteshamzadeh, M.; Hosseini, M. Effect of carbon steel microstructures and molecular structure of two new Schiff base compounds on inhibition performance in 1 M HCl solution by EIS. *Mater. Chem. Phys.* **2009**, *115* (2–3), 852–858.
- (11) Behpour, M.; Ghoreishi, S.; Soltani, N.; Salavati-Niasari, M.; Hamadani, M.; Gandomi, A. Electrochemical and theoretical investigation on the corrosion inhibition of mild steel by thiosalicylaldehyde derivatives in hydrochloric acid solution. *Corros. Sci.* **2008**, *50* (8), 2172–2181.
- (12) Leçe, H. D.; Emregül, K. C.; Atakol, O. Difference in the inhibitive effect of some Schiff base compounds containing oxygen, nitrogen and sulfur donors. *Corros. Sci.* **2008**, *50* (5), 1460–1468.
- (13) Sethi, T.; Chaturvedi, A.; Upadhyay, R.; Mathur, S. Corrosion inhibitory effects of some Schiff's bases on mild steel in acid media. *J. Chil. Chem. Soc.* **2007**, *52* (3), 1206–1213.
- (14) EL Basiony, N. M.; Elgendy, A.; Nady, H.; Migahed, M.; Zaki, E. Adsorption characteristics and inhibition effect of two Schiff base compounds on corrosion of mild steel in 0.5 M HCl solution: experimental, DFT studies, and Monte Carlo simulation. *RSC Adv.* **2019**, *9* (19), 10473–10485.
- (15) Ashmawy, A. M.; El-Sawy, A. M.; Khalil, H. F. Synthesis of novel liquid crystal compound and study of its behavior as corrosion inhibitor for mild steel in acidic medium (1 M) HCl. *Mol. Cryst. Liq. Cryst.* **2022**, *736* (1), 9–29.
- (16) Singh, A. K.; Singh, M.; Thakur, S.; Pani, B.; Kaya, S.; Ibrahim, B. E.; Marzouki, R. Adsorption study of N-(benzo [d] thiazol-2-yl)-1-(thiophene-2-yl) methanimine at mild steel/aqueous H<sub>2</sub>SO<sub>4</sub> interface. *Surf. Interfaces* **2022**, *33*, No. 102169.
- (17) Singh, A. K.; Chugh, B.; Singh, M.; Thakur, S.; Pani, B.; Guo, L.; Kaya, S.; Serdaroglu, G. Hydroxy phenyl hydrazides and their role as corrosion impeding agent: A detail experimental and theoretical study. *J. Mol. Liq.* **2021**, *330*, No. 115605.
- (18) Chugh, B.; Singh, A. K.; Thakur, S.; Pani, B.; Lgaz, H.; Chung, I.-M.; Jha, R.; Ebenso, E. E. Comparative investigation of corrosion-mitigating behavior of thiadiazole-derived bis-schiff bases for mild steel in acid medium: experimental, theoretical, and surface study. *ACS Omega* **2020**, *5* (23), 13503–13520.
- (19) Singh, A. K.; Chugh, B.; Thakur, S.; Pani, B.; Lgaz, H.; Chung, I.-M.; Pal, S.; Prakash, R. Green approach of synthesis of thiazolyl imines and their impeding behavior against corrosion of mild steel in acid medium. *Colloids Surf., A* **2020**, *599*, No. 124824.
- (20) Chugh, B.; Singh, A. K.; Poddar, D.; Thakur, S.; Pani, B.; Jain, P. Relation of degree of substitution and metal protecting ability of cinnamaldehyde modified chitosan. *Carbohydr. Polym.* **2020**, *234*, No. 115945.
- (21) Chugh, B.; Singh, A. K.; Chaouiki, A.; Salghi, R.; Thakur, S.; Pani, B. A comprehensive study about anti-corrosion behaviour of pyrazine carbohydrazide: Gravimetric, electrochemical, surface and theoretical study. *J. Mol. Liq.* **2020**, *299*, No. 112160.
- (22) Chugh, B.; Singh, A. K.; Thakur, S.; Pani, B.; Pandey, A. K.; Lgaz, H.; Chung, I.-M.; Ebenso, E. E. An exploration about the interaction of mild steel with hydrochloric acid in the presence of N-(Benzo [d] thiazole-2-yl)-1-phenylethan-1-imines. *J. Phys. Chem. C* **2019**, *123* (37), 22897–22917.
- (23) Singh, A. K.; Thakur, S.; Pani, B.; Chugh, B.; Lgaz, H.; Chung, I.-M.; Chaubey, P.; Pandey, A. K.; Singh, J. Solvent-free microwave assisted synthesis and corrosion inhibition study of a series of hydrazones derived from thiophene derivatives: Experimental, surface and theoretical study. *J. Mol. Liq.* **2019**, *283*, 788–803.
- (24) Upadhyay, A.; Purohit, A. K.; Mahakur, G.; Dash, S.; Kar, P. K. Verification of corrosion inhibition of Mild steel by some 4-Aminoantipyrine-based Schiff bases – Impact of adsorbate substituent and cross-conjugation. *J. Mol. Liq.* **2021**, *333*, No. 115960.
- (25) Metals, A. C. G.-o. C. o. *Standard Practice For Preparing, Cleaning, and Evaluating Corrosion Test Specimens*; ASTM International, 2017.
- (26) Deghadi, R. G.; Elsharkawy, A. E.; Ashmawy, A. M.; Mohamed, G. G. Can One Novel Series of Transition Metal Complexes of Oxydianiline Schiff Base Afford Advances in Both Biological Inorganic Chemistry and Materials Science? *Comments Inorg. Chem.* **2022**, *42* (1), 1–46.
- (27) Deghadi, R. G.; Elsharkawy, A. E.; Ashmawy, A. M.; Mohamed, G. G. Antibacterial and anticorrosion behavior of bioactive complexes of selected transition metal ions with new 2-acetylpyridine Schiff base. *Appl. Organomet. Chem.* **2022**, *36* (4), No. e6579.
- (28) Deyab, M. A.; Ashmawy, A. M.; Nessim, M. I.; Mohsen, Q. New Gemini surfactants based on alkyl benzenaminium: Synthesis and links to application of corrosion protection. *J. Mol. Liq.* **2021**, *332*, No. 115855.
- (29) Kamal, A.-B.; Mostfa, M. A.; Ashmawy, A. M.; El-Gaby, M. S. A.; Ali, G. A. M. Corrosion inhibition behavior of the synthesized pyrazoline-sulfonamide hybrid of mild steel in aqueous solutions: experimental and quantum investigations. *J. Chem. Sci.* **2022**, *134* (3), No. 90.
- (30) Wei, J.; Zhang, W.; Pan, W.; Li, C.; Sun, W. Experimental and theoretical investigations on Se (IV) and Se (VI) adsorption to UiO-66-based metal–organic frameworks. *Environ. Sci.: Nano* **2018**, *5* (6), 1441–1453.
- (31) Gad, E. A.; Azzam, E.; Halim, S. A. Theoretical approach for the performance of 4-mercapto-1-alkylpyridin-1-ium bromide as corrosion inhibitors using DFT. *Egyptian journal of petroleum* **2018**, *27* (4), 695–699.
- (32) Deyab, M. A.; Moustafa, Y. M.; Nessim, M. I.; Fathallah, N. A.; Asaad Bagato, N. M. New series of ionic liquids based on benzalkonium chloride derivatives: Synthesis, characterizations, and applications. *J. Mol. Liq.* **2020**, *313*, No. 113566.
- (33) Brycki, B.; Malecka, I.; Koziróg, A.; Otlewska, A. Synthesis, structure and antimicrobial properties of novel benzalkonium chloride analogues with pyridine rings. *Molecules* **2017**, *22* (1), 130.
- (34) Mohamed, A. I. A.; Sultan, A. S.; Hussein, I. A.; Al-Muntasheri, G. A. Influence of surfactant structure on the stability of water-in-oil emulsions under high-temperature high-salinity conditions. *J. Chem.* **2017**, *2017*, No. 5471376, DOI: 10.1155/2017/5471376.
- (35) Kuş, E.; Mansfeld, F. An evaluation of the electrochemical frequency modulation (EFM) technique. *Corros. Sci.* **2006**, *48* (4), 965–979.
- (36) Abdel-Rehim, S.; Khaled, K.; Abd-Elshafi, N. Electrochemical frequency modulation as a new technique for monitoring corrosion

inhibition of iron in acid media by new thiourea derivative. *Electrochim. Acta* **2006**, *51* (16), 3269–3277.

(37) Deyab, M.; Ashmawy, A. M.; Nessim, M.; Mohsen, Q. New Gemini surfactants based on alkyl benzenaminium: Synthesis and links to application of corrosion protection. *J. Mol. Liq.* **2021**, *332*, No. 115855.

(38) Khaled, K.; Hackerman, N. Investigation of the inhibitive effect of ortho-substituted anilines on corrosion of iron in 1 M HCl solutions. *Electrochim. Acta* **2003**, *48* (19), 2715–2723.

(39) Deyab, M.; Abd El-Rehim, S.; Keera, S. Study of the effect of association between anionic surfactant and neutral copolymer on the corrosion behaviour of carbon steel in cyclohexane propionic acid. *Colloids Surf., A* **2009**, *348* (1–3), 170–176.

(40) Deyab, M.; Keera, S. Effect of nano-TiO<sub>2</sub> particles size on the corrosion resistance of alkyd coating. *Mater. Chem. Phys.* **2014**, *146* (3), 406–411.

(41) Emregül, K. C.; Atakol, O. Corrosion inhibition of mild steel with Schiff base compounds in 1 M HCl. *Mater. Chem. Phys.* **2003**, *82* (1), 188–193.

(42) Asan, A.; Kabasakaloglu, M.; Işıklan, M.; Kılıç, Z. Corrosion inhibition of brass in presence of terdentate ligands in chloride solution. *Corros. Sci.* **2005**, *47* (6), 1534–1544.

(43) Stanly Jacob, K.; Parameswaran, G. Corrosion inhibition of mild steel in hydrochloric acid solution by Schiff base furoin thiosemicarbazone. *Corros. Sci.* **2010**, *52* (1), 224–228.

(44) Lgamri, A.; Abou El Makarim, H.; Guenbour, A.; Bachir, A. B.; Aries, L.; El Hajjaji, S. Electrochemical study of the corrosion behaviour of iron in presence of new inhibitor in 1 M HCl. *Prog. Org. Coat.* **2003**, *48* (1), 63–70.

(45) Singh, A. K.; Ebenso, E. E. Effect of Ceftezole on the corrosion of mild steel in HCl solution. *Int. J. Electrochem. Sci.* **2012**, *7*, 2349–2360.

(46) El-Taib Heakal, F.; Deyab, M.; Osman, M.; Nessim, M.; Elkholy, A. Synthesis and assessment of new cationic gemini surfactants as inhibitors for carbon steel corrosion in oilfield water. *RSC Adv.* **2017**, *7* (75), 47335–47352.

(47) Jeeva, M.; susai Boobalan, M.; Prabhu, G. V. Adsorption and anticorrosion behavior of 1-((pyridin-2-ylamino)(pyridin-4-yl) methyl) pyrrolidine-2, 5-dione on mild steel surface in hydrochloric acid solution. *Res. Chem. Intermed.* **2018**, *44* (1), 425–454.

(48) Kumar, C. B. P.; Mohana, K. N.; Muralidhara, H. B. Electrochemical and thermodynamic studies to evaluate the inhibition effect of synthesized piperidine derivatives on the corrosion of mild steel in acidic medium. *Ionics* **2015**, *21* (1), 263–281.

(49) Quartarone, G.; Battilana, M.; Bonaldo, L.; Tortato, T. Investigation of the inhibition effect of indole-3-carboxylic acid on the copper corrosion in 0.5 M H<sub>2</sub>SO<sub>4</sub>. *Corros. Sci.* **2008**, *50* (12), 3467–3474.

(50) Hegazy, M.; El-Tabei, A.; Bedair, A.; Sadeq, M. An investigation of three novel nonionic surfactants as corrosion inhibitor for carbon steel in 0.5 M H<sub>2</sub>SO<sub>4</sub>. *Corros. Sci.* **2012**, *54*, 219–230.

(51) Yadav, D. K.; Quraishi, M.; Maiti, B. Inhibition effect of some benzylidenes on mild steel in 1 M HCl: an experimental and theoretical correlation. *Corros. Sci.* **2012**, *55*, 254–266.

(52) Zhang, S.; Tao, Z.; Liao, S.; Wu, F. Substitutional adsorption isotherms and corrosion inhibitive properties of some oxadiazolotriazole derivative in acidic solution. *Corros. Sci.* **2010**, *52* (9), 3126–3132.

(53) Abd El-Rehim, S. S.; Hassan, H. H.; Deyab, M. A. M.; Abd El Moneim, A. Experimental and theoretical investigations of adsorption and inhibitive properties of Tween 80 on corrosion of aluminum alloy (A5754) in alkaline media. *Z. Phys. Chem.* **2016**, *230* (1), 67–78.

(54) Gad, E. A.; Al-Fahemi, J. H. Adsorptivity and corrosion inhibition performance of 2-(alkyloxy)-N, N, N-tris (2-hydroxyethyl)-2-oxo-ethanaminium chloride using DFT Approach. *Int. J. Sci. Eng. Res.* **2015**, *6*, 570–576.

(55) Binsi, M. P.; Joby, T.; Ragi, K.; Sini, V.; Reeja, J. Interaction of two heterocyclic Schiff bases derived from 2-acetyl pyridine on mild

steel in hydrochloric acid: Physicochemical and corrosion inhibition investigations. *Curr. Chem. Lett.* **2020**, *9* (1), 19–30.

(56) Ramesh, S.; Adhikari, A. V. Corrosion inhibition of mild steel in acid media by quinolinyl thiopropano hydrazone. *Indian J. Chem. Technol.* **2009**, *16* (2), 162–174.